

# Inverse planning anatomy-based dose optimization for HDR-brachytherapy of the prostate using fast simulated annealing algorithm and dedicated objective function

Etienne Lessard<sup>a)</sup>

*Service de radio-oncologie, L'Hôtel-Dieu de Québec, Centre Hospitalier Universitaire de Québec (CHUQ),  
Centre de recherche en cancérologie de l'Université Laval, 11 Côte du Palais, Québec,  
G1R 2J6, Canada*

Jean Pouliot

*Department of Radiation Oncology, University of California in San Francisco (UCSF), 505, Parnassus  
Avenue, San Francisco, California 94143*

(Received 7 August 2000; accepted for publication 26 February 2001)

An anatomy-based dose optimization algorithm is developed to automatically and rapidly produce a highly conformal dose coverage of the target volume while minimizing urethra, bladder, and rectal doses in the delivery of an high dose-rate (HDR) brachytherapy boost for the treatment of prostate cancer. The dwell times are optimized using an inverse planning simulated annealing algorithm (IPSA) governed entirely from the anatomy extracted from a CT and by a dedicated objective function (cost function) reflecting clinical prescription and constraints. With this inverse planning approach, the focus is on the physician's prescription and constraint instead of on the technical limitations. Consequently, the physician's control on the treatment is improved. The capacity of this algorithm to represent the physician's prescription is presented for a clinical prostate case. The computation time (CPU) for IPSA optimization is less than 1 min (41 s for 142 915 iterations) for a typical clinical case, allowing fast and practical dose optimization. The achievement of highly conformal dose coverage to the target volume opens the possibility to deliver a higher dose to the prostate without inducing overdosage of urethra and normal tissues surrounding the prostate. Moreover, using the same concept, it will be possible to deliver a boost dose to a delimited tumor volume within the prostate. Finally, this method can be easily extended to other anatomical sites. © 2001 American Association of Physicists in Medicine.  
[DOI: 10.1118/1.1368127]

Key words: inverse planning, brachytherapy, HDR, prostate, simulated annealing

## I. INTRODUCTION

The last decade has seen major changes in the way radiation treatments are delivered. The century-old objective of radiation therapy, i.e., to deliver a curative dose to the target while preserving normal tissues, can now be aimed at with a high degree of sophistication. However, in spite of major improvements achieved with 3D imaging modalities that allow the anatomy to be properly defined, brachytherapy treatments have not yet fully benefit from these important new pieces of information. The positioning of the seeds for permanent implant or of catheters for after-loading treatment is now image guided, greatly improving the localization of the applicators. At the planning stage, however, the anatomy is usually only indirectly taken into account. For high dose-rate (HDR) brachytherapy, catheters are placed in the target volume and it is assumed that if the dose distribution covers the catheters, it should also cover the anatomy. Imaging is commonly used to set the treatment margins, but optimized dose distributions are based on considerations such as catheter positions and desired dose to a few defined points. This necessarily results in an approximation of the shape of the anatomy. For the case of treatment of the prostate, volume optimization results in a dose distribution that is essentially

cylindrical in shape. This may represent an "average" prostate, but each prostate has a very specific shape. Any approximation of its shape to a geometrical representation will result in an overdosage of normal tissues surrounding the prostate. The organs at risk in the vicinity of the prostate may be included in this unnecessarily overdosed region.

Recent studies<sup>1</sup> indicated that the treatment of the prostate with a 3–5 mm margin by brachytherapy would encompass all known disease in 99%–100% of the specimens with extraprostatic extension. A cylindrical approximation of the shape of the prostate is not able to assure the complete coverage of the prostate volume. Only a conformal dose distribution to the anatomy with adequate margin around the prostate will encompass all disease.

Furthermore, Brenner and Hall<sup>2</sup> mentioned that for prostate cancer, the tumor and the surrounding late-responding tissues are likely to have similar  $\alpha/\beta$  values, and thus similar sensitivities to changes in fractionation. Consequently, fractionation will neither significantly increase nor decrease the therapeutic advantage between tumor control and late sequel. The result is that the healthy tissue can be only spared by the reduction of the dose. On the other hand, increasing radiation dose to the tumor improves local tumor control and

survival.<sup>3,4</sup> The only way to increase the dose to the tumor without delivering more dose to the healthy tissues is to be conformal. Thus the reach of highly conformal dose coverage for prostate cancer treatment is of major importance.

In the same paper, Brenner and Hall<sup>2</sup> concluded: "High dose-rate (HDR) brachytherapy would be highly appropriate modality for treating prostate cancer. Appropriately designed HDR-brachytherapy regimens would be expected to be as efficacious as low dose rate, but with added advantages of logistic convenience and more reliable dose distribution." With modern imaging modalities and fast computers now available, tools are at hand to develop a planning method that can provide highly conformal dose coverage using all the potential of HDR-brachytherapy.

In previous work on permanent implant for the treatment of prostate cancer,<sup>5,6</sup> we developed a computer program based on a fast simulated annealing algorithm to automatically and rapidly produce plans for the treatment. We have shown that this dose optimization, when properly tuned, has the potential to deliver highly conformal and robust plans.<sup>7</sup> Moreover, once parameters controlling the iteration process are properly tuned, automatic dose distributions can be optimized within 2 to 3 min for a complete range of prostate sizes and shapes with no further patient-to-patient parameter adjustment. This optimization is now routinely used clinically.

The optimization process used to compute the seed positions is guided by the dose coverage and dose constraints specified by the radiation oncologist on the anatomy extracted from ultrasound images. Instead of defining the treatment configuration to distribute the dose to agree with the physician's prescription, our approach uses the physician's prescription to guide the optimization toward the best treatment configuration. This change of perspective is called inverse planning. With this new approach, the focus is on the physician's prescription and constraint instead of on the technical limitations. Consequently, the physician's control on the treatment is improved.

The goal of this paper is to apply the concept of inverse planning to obtain an anatomy-based optimization of the dose distribution without any manual modification to deliver a highly conformal HDR prostate treatment. Knowing the exact localization of the applicators, owing to modern imaging modalities, it is easy to establish the possible stopping position of the radioactive source. Given  $j$  possible source positions (dwell positions) the problem is the determination of  $j$  times (dwell times) so that the resulting dose distribution will closely respect the clinical criteria. Those criteria are included in a dedicated objective function, known as the cost function, to govern an optimization process. We will introduce an HDR inverse planning dose optimization governed entirely from the anatomy and clinical criteria to decide the best dwell time distribution. After a brief description of the procedure and of the inverse planning simulated annealing (IPSA) algorithm, results obtained for different optimization parameters are presented. This will provide an opportunity to evaluate the capability of the algorithm to meet the physician's prescription.

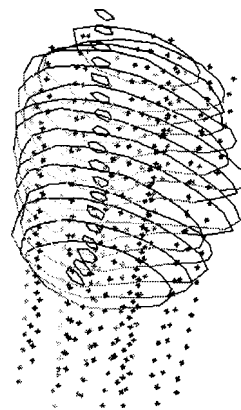


FIG. 1. Anatomical contours and dwell positions extracted from CT.

## II. TREATMENT PROCEDURE

The treatment of prostate cancer with HDR radiation therapy involves several steps.<sup>8</sup> Only those relevant to dose planning will be presented. Once a patient has been selected for HDR treatment, catheters are inserted in his prostate through the perineum. This is performed under ultrasound guidance in the operating room. An often cited advantage of HDR over permanent implants is that dose distribution is calculated after catheters are in place. Usually, a total of 18 catheters are needed to offer sufficient dwell time positions to cover the entire prostate.

A CT is then obtained with the patient in supine position. Anatomical structures (prostate, bladder, urethra, rectum, etc.) and dwell positions are digitized for use at the planning time (Fig. 1). The planning process involves the use of this information to define dwell time values to produce a clinically acceptable dose distribution. The catheters in the prostate will then be attached to the after-loading unit (Nucletron MicroSelectron-High Dose Rate Remote Afterloader) for treatment delivery according to the computed dwell time distribution. Our current method calls for a single interstitial prostate implant with three subsequent Ir<sup>192</sup> HDR fractions.

The optimization routine used to determine the dwell time distribution minimizes a dedicated objective function (cost function) that mathematically describes the clinical objective (the smaller the cost function, the closer to the clinical objective). A few algorithms have been based on the same concept.<sup>9,10</sup> In the former, however, the use of a simplex algorithm cannot guarantee that the solution found is optimal and has been tested on simple geometrical volume. In the latter case, computing time needed for optimization strongly limits clinical applications. The fast-simulated annealing algorithm can be used to overcome these problems.

## III. SIMULATED ANNEALING

An optimization technique allowing for wider sampling and hill climbing to escape from a local minimum is required whenever the cost function is mathematically nonlinear and therefore presents multiple minimums. Simulated annealing (SA), first introduced by Kirkpatrick<sup>11</sup> and other related algorithms (Fast SA, Very Fast SA, or others<sup>12,13</sup>) are optimi-

zation techniques that can process cost functions with arbitrary boundary conditions with the statistical guarantee of finding an optimal solution. Equally important, SA class algorithms are easily coded compared to other nonlinear optimization algorithms. A multitude of problems arising from very different fields has been solved using SA algorithm.<sup>14</sup> In radiation therapy, this technique can be used to define the parameters of an external beam treatment.<sup>12,15</sup> This approach has been successfully adapted to brachytherapy to optimize the dose distribution of up to ten seeds in a cylindrical vaginal vault applicator (20 possible positions).<sup>16</sup> In our previous work,<sup>5,6</sup> we showed that the fast-simulated annealing algorithm can be used to govern a optimization process to automatically and rapidly produce plan for prostate permanent implant treatment. The excellent results obtained by this optimization have encouraged us to extend the same concept to after loading HDR prostate treatments.

### A. Algorithm runs

The optimization routine for HDR prostate treatments start with initial dwell times values uniformly set to 1 s. Although this choice of dwell time values is purely arbitrary and the algorithm produces a final result independent of starting values, we felt it was reasonable to assign initial dwell times with realistic values.

Beginning with this initial dwell time distribution at Step  $k$  (the current one), a transition is generated (Step  $k+1$ ) by randomly incrementing or decreasing on random chosen dwell times ( $\pm 0.1$  s). At each iteration, the algorithm must decide if the new dwell time distribution is accepted to become the current one and replace the former distribution. The decision criterion used is based on the cost function values for the two arrangements:  $E_{k+1}$  and  $E_k$ . The probability  $P(\Delta E)$  of accepting the transition depends on the difference  $\Delta E = E_{k+1} - E_k$ . For a transition resulting in a lower value of the cost function ( $\Delta E < 0$ ), the new distribution is always accepted as the current one. A change that results in an increase of the cost function, ( $\Delta E > 0$ ), is accepted with a probability given by

$$P(\Delta E) = \exp[-\Delta E/T(k)], \quad (1)$$

where  $T(k)$  is the pseudo-temperature parameter. Thus for a given positive  $\Delta E$ , transitions are accepted more easily at higher temperatures, which permit the system to escape from local minimum with a finite probability. The temperature parameter  $T(k)$  is reduced at each Step  $k$  until the system no longer evolves. In the case where  $T$  would be set to zero for all  $k$ , the probability of accepting a transition with a positive  $\Delta E$  would be zero and the optimization would behave as a regular local search algorithm.

### B. Cooling schedule

In the analogy of the simulated annealing schedule typical of standard SA, the pseudo-temperature is decreased only after a large number of distributions have been tested, assuring that thermal equilibrium has been reached, at least statistically. This approach gives consistent results in the search of

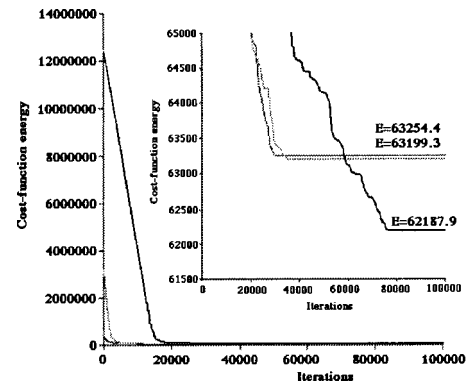


FIG. 2. Result of optimization by means of a local search algorithm: The three curves differ only by their initial dwell time distribution. Energy units are arbitrary.

the global minimum. However, as stated in the literature, standard SA tends to be too slow.<sup>14</sup> The fast-simulated annealing (FSA) used here differs from SA and can be used as an alternative to standard SA: The temperature parameter  $T(k)$  used to calculate  $P(\Delta E)$  is reduced at every iteration according to the relation

$$T(k) = T_0/k^\alpha, \quad (2)$$

where  $k$  is the iteration number,  $T_0$  the initial temperature, and  $\alpha$  the speed parameter. The initial pseudo-temperature is set proportional to the mean  $\Delta E$  values of 500 random transitions  $E(k)$  to  $E(k+1)$ . The speed parameter was empirically set to 0.6 to optimize the results on five prostates from clinical cases while preserving a reasonable time for clinical application. The cooling sequence is stopped when a large number of iterations (5000) have been performed without any change in the cost function value.

### C. Is simulated annealing really required?

Optimization by means of a local search algorithm cannot guarantee that the identified dwell time distribution will be the best distribution. To demonstrate this fact, we have performed three optimization on the same clinical case with a temperature set to zero. Setting  $T=0$  in Eq. (1) effectively transforms the optimization process into a strictly downhill algorithm. Figure 2 presents the values of these optimization at each iterations during the minimization process. The three curves represent calculations with different initial dwell time distributions. We observe three different solutions; the calculation stopped at a sub-optimal solution because no distribution with a lower cost function could be found nearby the current one. Clearly, the algorithm was trapped in a local minimum. Even though a local search algorithm may find a satisfactory clinical solution most of the time, it cannot insure that the optimization will not result on a sub-optimal solution for a specific case (prostate shape, catheter position, clinical constraint).

## IV. CONSTRAINTS AND COST FUNCTION

### A. Clinical criteria

A cost function is used to translate the clinical criteria into mathematical form. This cost function  $E(k)$  allows comparison of a given dwell time distribution  $k$  relative to the next  $k + 1$ . The clinical criteria used for the optimization are: (A) The delivery of a minimum prescribed peripheral dose (mPD) on prostate contours; (B) A uniform dose distribution within the planned target volume, i.e., no hot spot or cold spot; (C) A limited dose to the urethra; (D) A limited dose to the normal tissues around the prostate.

### B. Dose calculation points

The choice of the dose point locations can influence the optimization result. In a recent publication<sup>17</sup> it was suggested that uniformly distributed dose points on the PTV contours as a representation of the 3D PTV surface could give biased results, since they do not completely cover the whole PTV. Another report<sup>18</sup> concluded that an improper selection of a limited number of dose optimization points for the derivation of optimized dose distribution of HDR vaginal cylinder could affect the dose distributions. In our case, several hundred dose points are uniformly generated on the contours, extremities, and inside the target volume and organ at risks (criteria A, B, and C). Also, the cost function considers dose points uniformly distributed outside the target volume to impose criteria D (Fig. 3).

### C. Dose calculation and cost function

Knowing the dose calculation point and the dwell position coordinates, the dose-rate contribution from a dwell position  $j$  to a given dose calculation point  $i$ , is given by the following equation according to TG43:<sup>19</sup>

$$d_{ij} = S_k \Lambda \Phi_{an}(\theta, r_{ij}) g(r_{ij}) / r_{ij}^2, \quad (3)$$

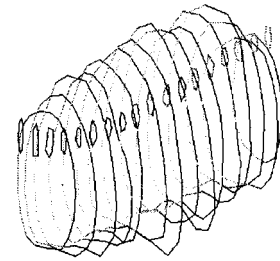
where  $S_k$  is the air kerma strength,  $\Lambda$  the dose-rate constant,  $\Phi_{an}(\theta, r_{ij})$  the anisotropy function,  $g(r_{ij})$  the radial dose function, and  $r_{ij}$  the distance between the dwell position  $j$  and the dose calculation point  $i$ . High dose contribution from dwell position very close to dose points is avoided by ignoring this dose point when  $r_{ij}$  is smaller than an adjustable cutoff value (default value is 2 mm).

From the dose-rate matrix  $d_{ij}$  obtained by Eq. (3), the calculation of the dose distribution  $D_i$  is given by the sum of the dose-rate contribution from all dwell positions  $j$  with a respective dwell time  $t_j$ :

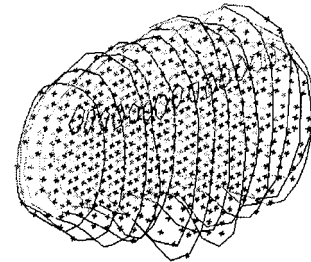
$$D_i = \sum_j d_{ij} t_j. \quad (4)$$

The degree of fulfilment of each clinical criterion is measured by the use of dose potentials. These dose potentials convert the dose distribution obtained by Eq. (4) to a penalty value  $w_i$ . This conversion is defined by the relation:

A)



B)



C)

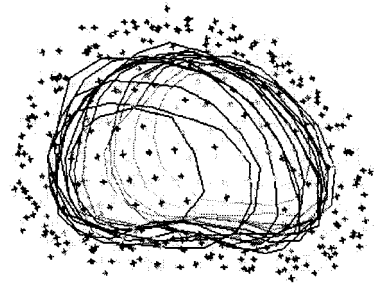


Fig. 3. Dose points. (A) Prostate and urethra contours. (B) Uniformity dose points. (C) External dose points.

$$w_i = \begin{cases} m_L(D_i - L) & \text{if } D_i < L \\ m_R(D_i - R) & \text{if } D_i > R \\ 0 & \text{if } L \leq D_i \leq R, \end{cases} \quad (5)$$

where the parameters  $m_L$ ,  $m_R$ ,  $L$ , and  $R$  are the characteristic of the selected dose potentials (Fig. 4). Each clinical criterion is controlled by its own potential active on its respective dose calculation points. Examples of potential chosen to fulfill the physician's prescription are shown in Fig. 5.

Finally, the sum of the penalty values  $w_i$  over  $m$  dose points is performed to obtain the global penalty  $E_n$  of a given clinical criterion  $n$ :

$$E_n = \sum_i^m \frac{w_i}{m}. \quad (6)$$

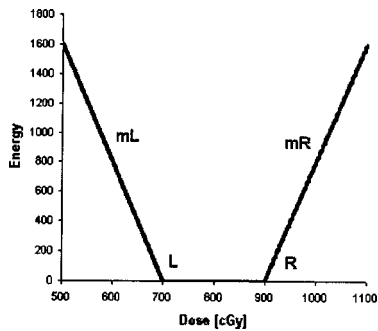


FIG. 4. Dose potential defined by the Eq. (5).

The cost function  $E(k)$  of the dwell time distribution of iteration  $k$  is given by the sum of all terms representing the clinical criteria:

$$E(k) = \sum_{n=1}^4 E_n(k). \quad (7)$$

This energy value is used to compare a given dwell time distribution  $k$  relative to the next  $k+1$ . The closer to the clinical objective and to the physician's prescription, the smaller the energy and the cost function. Agreement with the physician's prescription and the importance of a clinical criterion over the other is adjusted using the parameters of the dose potentials. Thus the most sensitive part of the algorithm is the choice these parameters.

#### D. Automatic activation of source dwell positions

The final dose distribution obtained with conventional dose optimization algorithms strongly depends on the appropriate selection of source dwell positions. The manual selection of dwell positions (200 positions on average) with a trial and error strategy can be time-consuming.<sup>20</sup> Furthermore, the

effectiveness of the manual method strongly depends on the dosimetrist experience. In our case, the rapidly falling dose constraint in normal tissues surrounding the prostate and the limited dose constraint on the urethra automatically switches off the undesirable dwell positions (dwell time=0). Furthermore, to reduce the CPU time, dwell positions outside of a margin around the prostate are automatically excluded from the research space prior to starting the optimization. To optimize, the algorithm needs only prostate and urethra contours points, catheter dwell positions, and the physician's prescription described by the dose potentials.

## V. RESULTS

To illustrate the flexibility of the IPSA algorithm, several plannings from the same clinical prostate case (23 cc) were obtained using different dose potential parameters. The catheters were peripherally distributed like every implant performed at our center. The resulting isodose distributions for a given plane and DVH are presented in Figs. 6 and 7, respectively.

In Fig. 6(A, B, C), the small darker area shown in the middle represents the urethra and the numbers show the dwell time and catheter numbers. The third isodose from outside corresponds to the prescribed dose of the 100% isodose (6 Gy). Other isodoses are 1 Gy apart.

The first isodose distribution [Fig. 6(A)] is the result obtained with the dose potential presented in Fig. 5 used to fulfill the clinical criteria. One can clearly see that the isodose resulting from the IPSA optimization is conformal. This is the result of the prostate contour-dose potential in the cost function. Also, a fast fall off of the high doses inside the target volume could be observed on the prostate DVH [Fig. 7(A)], due to the uniformity-dose potential.

Results are presented in Figs. 6(B) and 6(C) for two other sets of parameters. For case B, the maximum inside-dose is

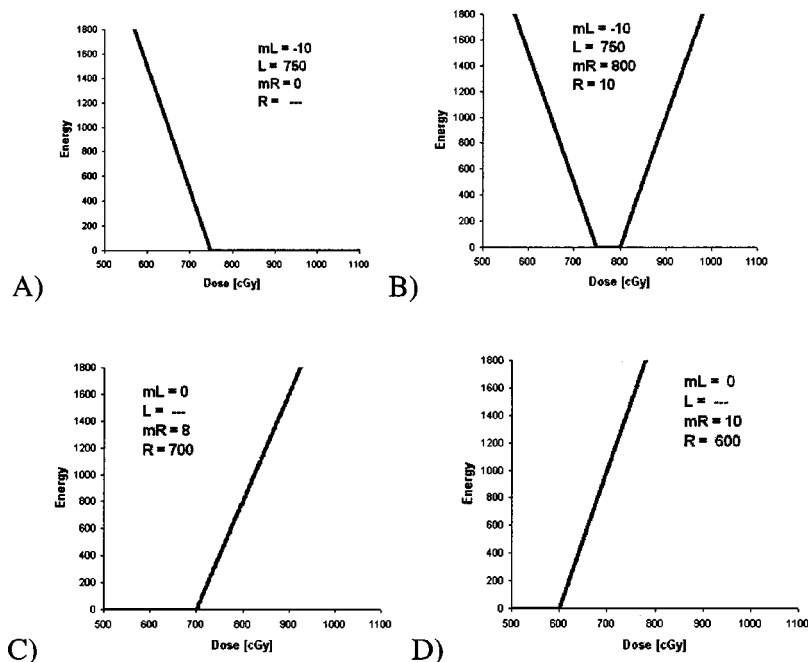


FIG. 5. Potentials chosen to respect the physician's prescription. Prostate contour—dose potential. (A) Uniformity—dose potential. (B) Urethra—dose potential. (C) External—dose potential. (D).

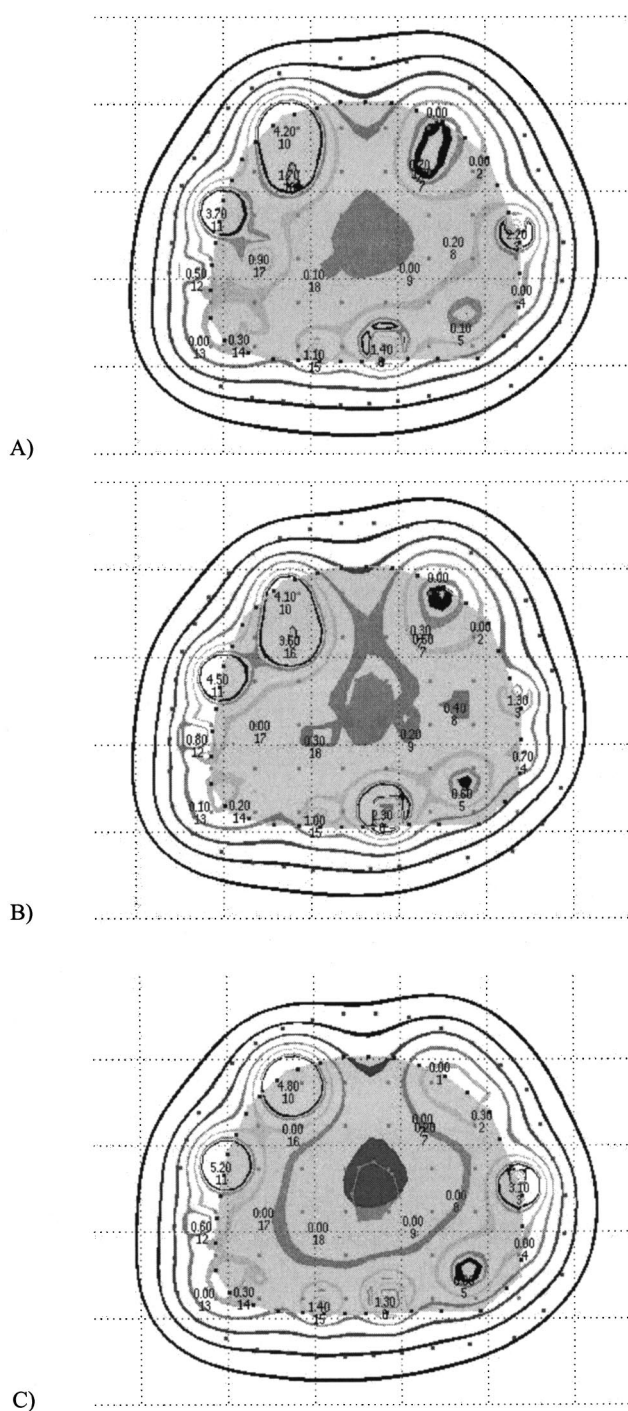


FIG. 6. Isodose distribution of plane #3 obtained from (A) dose potentials from Fig. 5, (B) Harder on uniformity—dose potential, (C) Harder on urethra—dose potential.

set to 750 cGy rather than 800 cGy [as in Fig. 6(A)]. The resulting dose distribution is cooler inside the prostate and the peripheral margin is reduced [Fig. 6(B)]. However, this modification results in a faster fall off of the high dose [Fig. 7(A)]. Also, if the maximum dose on the urethra is set to 600 cGy rather than 700 cGy [Fig. 6(A)], the resulting dose distribution is clearly cooler on the urethra [Fig. 6(C)]. Furthermore, the urethra DVH shows the direct relation between the

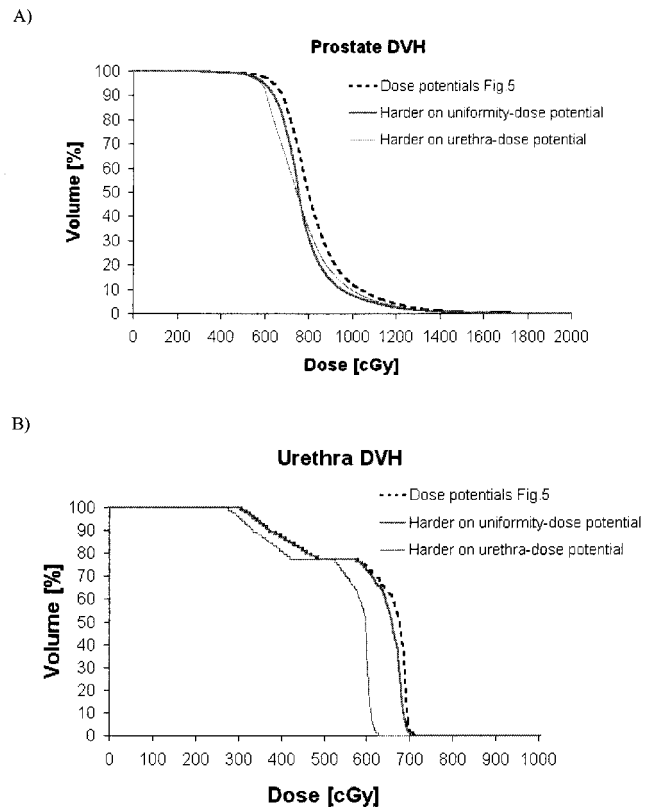


FIG. 7. Prostate (A) and urethra (B) DVH presented for different dose potential sets.

constraints and the results [Fig. 7(B)]. Those examples give a good idea of the flexibility of the cost function.

A publication on the relationship between hot spots and complications following HDR<sup>21</sup> concludes that dose heterogeneity appeared to be rather unimportant with regard to complication. Consequently, the importance of the dose uniformity over the urethra protection can be lower. However, the choice of the dose potential parameters is a clinical decision. Consequently, the physicians directly control the treatment.

The computation time (CPU) for the IPSA dose optimization was less than 1 min (41 s for 142 915 iterations) for this typical case on a Pentium III (700 MHz). The running time depends on the quantity of dwell positions and dose points. For this typical case, 136 dwell positions were activated out of 198 possible dwell positions. A total of 1232 dose points were generated for the optimization purpose. The dose points were distributed as follow: 1099 dose points for the target (404 on the contours, 291 inside and 404 outside) and 133 for the urethra (52 on the contours and 81 inside).

## VI. CONCLUSION

We have developed an inverse planning dose optimization governed entirely from the anatomy and the physician's prescription for the treatment planning of prostate cancer with high dose-rate brachytherapy. With this inverse planning approach, the focus is on the physician's prescription and dose constraints instead on the technical limitations. Conse-

quently, the physician's control on the treatment is improved. The algorithm can automatically and rapidly generate a treatment plan (dwell time distribution) with reduced dose to organs at risk and normal tissue while providing a better conformal dose distribution around the target.

We have shown that the fast-simulated annealing algorithm can be used to govern the optimization process and insures that it is not stopped at a sub-optimal level. Equally important, this algorithm provides a dose distribution in less than 1 min of CPU time, allowing fast and practical dose optimization. The optimization is therefore achieved in a short time for clinical applications, insuring that the best quality of planning is independent of the dosimetrist experience. It will also produce a planning consistent between patients, providing patients the best planning and allowing comparisons between them.

The achievement of highly conformal dose coverage to the target volume opens the possibility to deliver a higher dose to the prostate without inducing overdosage of urethra and normal tissues surrounding the prostate. Moreover, using the same concept, it will be possible to deliver a boost dose to a delimited tumor volume within the prostate. Finally, this method can be easily extended to other anatomical sites.

## ACKNOWLEDGMENTS

We acknowledge financial support from the National Cancer Institute of Canada (NCIC) with funds from the Canadian Cancer Society and from Le Fonds pour la formation de Chercheurs l'Aide à la recherche (Fonds FCAR-Québec). The authors also want to acknowledge Bernard Lachance and Dr. Eric Vigneault (C.H.U.Q.) and Dr. I-Chow Hsu (U.C.S.F.) for fruitful discussions.

<sup>a)</sup>Present address: Department of Radiation Oncology, University of California in San Francisco (UCSF), 505, Parnassus Avenue, San Francisco, CA 94143, e-mail: lessard@radonc17.ucsf.edu

<sup>1</sup>B. J. Davis, T. M. Pisansky, T. M. Wilson, H. J. Rothenberg, A. Pacelli, D. W. Hillman, D. J. Sargent, and D. G. Bostwick, "The radial distance of extraprostatic extension of prostate carcinoma, implication for prostate brachytherapy," *American Cancer Society* **85**, 2630–2637 (1999).

<sup>2</sup>D. J. Brenner and E. J. Hall, "Fractionation and protraction for radiotherapy of prostate carcinoma," *Int. J. Radiat. Oncol., Biol., Phys.* **43**, 1095–1101 (1999).

<sup>3</sup>G. E. Hanks, A. L. Hanlon, W. H. Pinover, E. M. Horwitz, and T. E. Schultheiss, "Survival advantage for prostate cancer patients treated with high dose three-dimensional conformal radiotherapy," *Cancer J. Sci. Am.* **5**, 152–158 (1999).

<sup>4</sup>D. J. Brenner and E. J. Hall, "Fractionation and protraction for radiotherapy of prostate carcinoma," *Int. J. Radiat. Oncol., Biol., Phys.* **43**, 1095–1101 (1999).

<sup>5</sup>J. Pouliot, R. Taschereau, C. Coté, J. Roy, and D. Tremblay, "Dosimetric aspects of permanent radioactive implants for the treatment of prostate," *Physics in Canada* **55**, 61–68 (1999).

<sup>6</sup>J. Pouliot, D. Tremblay, J. Roy, and S. Filice, "Optimization of permanent <sup>125</sup>I prostate implants using fast simulated annealing," *Int. J. Radiat. Oncol., Biol., Phys.* **36**, 711–720 (1996).

<sup>7</sup>R. Taschereau, J. Roy, and J. Pouliot, "Monte Carlo simulation of prostate implants to improve dosimetry and compare planning methods," *Med. Phys.* **26**, 1952–1959 (1999).

<sup>8</sup>T. Mate, J. E. Gottesman, J. Hatton, M. Gribble, and L. Van Hollebeke, "High dose rate afterloading <sup>192</sup>Iridium prostate brachytherapy: Feasibility report," *Int. J. Radiat. Oncol., Biol., Phys.* **41**, 525–533 (1998).

<sup>9</sup>P. Kneschaurek, W. Schiessl, and R. Wehrmann, "Volume-based dose optimization in brachytherapy," *Int. J. Radiat. Oncol., Biol., Phys.* **45**, 811–815 (1999).

<sup>10</sup>M. Lahanas, D. Baltas, and N. Zamboglou, "Anatomy-based three-dimensional dose optimization in brachytherapy using multiobjective genetic algorithms," *Med. Phys.* **26**, 1904–1918 (1999).

<sup>11</sup>S. Kirkpatrick, C. D. Gelatt, and P. M. Vecchi, "Optimization by simulated annealing," *Science* **220**, 671–680 (1983).

<sup>12</sup>S. M. Morril, K. S. Lam, R. G. Lane, M. Langer, and I. I. Rosen, "Very fast simulated reannealing in radiation therapy treatment plan optimization," *Int. J. Radiat. Oncol., Biol., Phys.* **31**, 179–188 (1995).

<sup>13</sup>H. Szu and R. Hartley, "Fast simulated annealing," *Phys. Lett. A* **122**, 157–162 (1987).

<sup>14</sup>L. Ingberg, "Simulated annealing: Practice vs theory," *J. Math. Comput. Modelling* **18**, 29–57 (1993).

<sup>15</sup>S. Webb, "Optimization by simulated annealing of three dimensional conformal treatment planning for radiation fields defined by a multileaf collimator," *Phys. Med. Biol.* **36**, 1201–1226 (1991).

<sup>16</sup>R. S. Sloboda, "Optimization of brachytherapy dose distributions by simulated annealing," *Med. Phys.* **19**, 955–964 (1992).

<sup>17</sup>M. Lahanas, D. Baltas, S. Giannouli, N. Milickovic, and N. Zamboglou, "Generation of uniformly distributed dose points for anatomy-based three-dimensional dose optimization methods in brachytherapy," *Med. Phys.* **27**, 1034–1046 (2000).

<sup>18</sup>Z. Li, C. Liu, and J. R. Palta, "Optimization dose distribution of a high dose rate vaginal cylinder," *Int. J. Radiat. Oncol., Biol., Phys.* **41**, 239–244 (1998).

<sup>19</sup>R. Nath, L. L. Anderson, G. Luxton, K. A. Weaver, J. F. Williamson, and A. S. Meigooni, "Dosimetry of interstitial brachytherapy sources: Recommendations of the AAPM Radiation Therapy Committee Task Group No. 43," *Med. Phys.* **22**, 209–234 (1995).

<sup>20</sup>S. Giannouli, N. Milickovic, D. Baltas, M. Lahanas, N. Uzunoglu, C. Kolotas, and N. Zamboglou, "Autoactivation of source dwell positions: A new tool for imaging based HDR brachytherapy treatment planning," *Med. Phys.* **27**, 2517–2520 (2000).

<sup>21</sup>B. Vikram, S. Deore, J. J. Beitler, B. Sood, E. Mullokandov, A. Kapulsky, and D. P. Fontenla, "The relationship between dose heterogeneity ('HOT SPOTS') and complications following high-dose rate brachytherapy," *Int. J. Radiat. Oncol., Biol., Phys.* **43**, 983–987 (1999).